Physica D 238 (2009) 1507–1523

Contents lists available at ScienceDirect

Physica D

journal homepage: www.elsevier.com/locate/physd

Almost-invariant sets and invariant manifolds — Connecting probabilistic and geometric descriptions of coherent structures in flows

Gary Froyland[a,*], Kathrin Padberg[b]

[a] School of Mathematics and Statistics, University of New South Wales, Sydney NSW 2052, Australia

[b] Institut für Wirtschaft und Verkehr, Technische Universität Dresden, 01062 Dresden, Germany

ARTICLE INFO

Article history:
Received 26 March 2008
Received in revised form
6 March 2009
Accepted 9 March 2009
Available online 18 March 2009
Communicated by V. Rom-Kedar

Keywords:
Almost-invariant set
Coherent structure
Finite-time Lyapunov exponent
Invariant manifold
Transfer operator
Transport

ABSTRACT

We study the transport and mixing properties of flows in a variety of settings, connecting the classical geometrical approach via invariant manifolds with a probabilistic approach via transfer operators. For non-divergent fluid-like flows, we demonstrate that eigenvectors of numerical transfer operators efficiently decompose the domain into invariant regions. For dissipative chaotic flows such a decomposition into invariant regions does not exist; instead, the transfer operator approach detects *almost*-invariant sets. We demonstrate numerically that the boundaries of these almost-invariant regions are predominantly comprised of segments of co-dimension 1 invariant manifolds. For a mixing periodically driven fluid-like flow we show that while sets bounded by stable and unstable manifolds are almost-invariant, the transfer operator approach can identify almost-invariant sets with smaller mass leakage. Thus the transport mechanism of lobe dynamics need not correspond to minimal transport.

The transfer operator approach is purely probabilistic; it directly determines those regions that minimally mix with their surroundings. The almost-invariant regions are identified via eigenvectors of a transfer operator and are ranked by the corresponding eigenvalues in the order of the sets' invariance or "leakiness". While we demonstrate that the almost-invariant sets are often bounded by segments of invariant manifolds, without such a ranking it is not at all clear *which* intersections of invariant manifolds form the major barriers to mixing. Furthermore, in some cases invariant manifolds do not bound sets of minimal leakage.

Our transfer operator constructions are very simple and fast to implement; they require a sample of short trajectories, followed by eigenvector calculations of a sparse matrix.

1. Introduction

Transport and mixing processes play an important role in many natural phenomena and their mathematical analysis has received considerable interest in the last two decades. Areas of application include astrodynamics, molecular dynamics, fluid dynamics, and ocean dynamics; see e.g. [1–4] for discussions of transport phenomena. Analytical and numerical treatments of transport typically assume that the motion of a passive particle is completely determined by an underlying autonomous or nonautonomous velocity field. A variety of different concepts from dynamical systems theory may then be used to detect barriers to particle transport, to explain the transport mechanisms at work, and to quantify transport in terms of transition rates or probabilities. Two different families of approaches have been developed in the past for the analysis of transport and mixing processes in dynamical systems: (i) *geometric* methods which make use of invariant manifolds and related concepts and (ii) *probabilistic* techniques which attempt to approximate so-called almost-invariant sets. One of the main aims of this work is to demonstrate numerically in a number of case studies that there is a strong connection between the two approaches and that the combination of the two types of analyses leads to a richer understanding of the global dynamics.

The notion that geometrical structures such as invariant manifolds play a key role in dynamical transport and mixing for fluid-like flows has been around for almost two decades. In autonomous settings, invariant cylinders and tori form impenetrable dynamical barriers. This follows directly from the uniqueness of trajectories of the underlying ordinary differential equation (ODE). Slow mixing and transport in periodically driven maps and flows can sometimes be explained by lobe dynamics of invariant manifolds [5,6,3]. In non-periodic time-dependent settings, finite-time hyperbolic material lines [7] and surfaces [8] have been proposed as barriers to mixing. Both the theoretical and the numerical analysis of these Lagrangian coherent structures in mixing fluids in many different application areas has been the focus of considerable interest over the last decade and a half, see e.g. [7–13], and the references therein.

Unions of segments of invariant manifolds may form either complete or partial boundaries of regions that are completely or

* Corresponding author. Tel.: +61 2 9385 7050; fax: +61 2 9385 7123.
E-mail address: g.froyland@unsw.edu.au (G. Froyland).

0167-2789/$ – see front matter
doi:10.1016/j.physd.2009.03.002

Probabilistic Description of Dynamics
Transfer Operator
Almost-invariant Sets

Identifies which geometric structures are the strongest barriers to global mixing $\downarrow$

$\uparrow$ Further informs the dynamics underlying almost-invariant sets

Geometric Description of Dynamics
Invariant Manifolds

Fig. 1. Connecting the probabilistic and the geometric approaches.

partially dynamically isolated. These dynamically isolated regions are either invariant sets or *almost-invariant* sets. One of the main aims of this work is to demonstrate numerically that the regions that are *maximally* almost-invariant often have boundaries comprised of segments of invariant manifolds.

Almost-invariant sets arose in the context of smooth maps and flows on subsets of $\mathbb{R}^d$ [14,15] about a decade ago. The main theoretical and computational tool is the Perron–Frobenius (or transfer) operator, and almost-invariant sets were estimated heuristically from eigenfunctions of the Perron–Frobenius operator. Further theoretical and computational extensions have since been constructed [16–18]. A parallel series of work specific to time-symmetric Markov processes and applied to identifying molecular conformations was developed in [19] and surveyed in [19,20]. The constructions of [20] are transfer operator based and the transfer operator is derived directly from ensemble simulation of the dynamics. Related ideas have also been developed for finite-state Markov chains [21,22], where the starting point is a Markov chain model of some physical system that is similar in spirit to a transfer operator.

Connections between eigenmodes of evolution operators and slow mixing in fluid flow have recently begun to appear. Liu and Haller [23] observe via simulation a transient "strange eigenmode" as predicted by classical Floquet theory. Pikovsky and Popovych [24,25] numerically integrated an advection–diffusion equation to simulate the evolution of a passive scalar, observing that it is the subdominant eigenmode of the corresponding transfer operator that describes the most persistent deviation from the unique steady state. The particular form of flow used in [24,25] admitted a convenient Fourier series representation that allowed calculation of leading eigenmodes. The numerical methods we describe in the present paper can be used to estimate eigenmodes for flows that are continuous in space and time and require only the calculation of many short trajectories.

Prior work related to connections between geometric and statistical objects include [26,27], where ergodic averages of observables have been used to identify *invariant* sets in autonomous and periodically driven fluid-like flows in two and three dimensions. Connections with finite-time invariant manifolds have been studied numerically in the aperiodically driven setting [28]. The approaches [26–28] have the disadvantages of (i) requiring possibly lengthy integration times and (ii) the ambiguity of selecting an observable to ergodically average. In contrast, our transfer operator approach employs relatively short integration times and directly constructs slow eigenmodes that carry information about invariant and almost-invariant sets. The first connection between almost-invariant sets and invariant manifolds appeared in [29], where graph algorithms were applied to analyse transport in astrodynamics. The present paper significantly extends the results of [29] by treating a wide variety of systems and framing the probabilistic approach in terms of eigenfunctions of transfer operators rather than graph partitioning. The spectral approach is more natural, especially under variation of initial flow times and flow durations and delivers significant benefits in terms of the transfer operator describing the global dynamics.

In this work via a number of case studies in two and three dimensions, for autonomous and time-periodic flows, and for fluid-like and dissipative flows, we compare the geometric, manifold based decomposition of the phase space with the decomposition provided by the transfer operator approach. We will show that the two approaches are largely compatible in the sense that the manifolds often form at least partial boundaries of the regions identified by the transfer operator approach. In such situations the methods are complementary: (see also Fig. 1)

- the probabilistic approach determines which regions are the most dynamically isolated and therefore which manifold intersections are the most important in defining the boundaries of such regions,
- recognising that the boundaries of the almost-invariant regions are pieces of invariant manifold allows a more detailed understanding of the dynamics near the boundaries of the sets and how transport occurs in and out of the almost-invariant regions.

An outline of this paper is as follows. In Section 2 we provide background definitions for invariant sets, invariant measures, and ergodic measures, and summarise the four dynamical settings we will investigate. In Section 3 we define almost-invariant sets and the Perron–Frobenius operator. We then describe our numerical method for producing a finite-rank approximation of the operator and detail an algorithm for using eigenvectors of this finite-rank operator to determine almost-invariant sets. In Section 4 we investigate the connection between the probabilistic description of coherent structures via almost-invariant sets and the geometric description using invariant manifolds. Sections 5–8 contain our four major case studies in which we demonstrate the efficiency of the transfer operator approach in determining and extracting the largest, most coherent structures. In each case study we additionally compute major geometrical structures and demonstrate a high degree of correlation between the geometric structures and the almost-invariant sets. We find one exception to this correlation in the second part of our final case study where we show that lobe related transport need not correspond to minimal leakage from a set.

2. Background: Flows, invariant sets, and invariant measures

Let $M \subset \mathbb{R}^d$ be compact and $F : M \times \mathbb{R} \to \mathbb{R}^d$ be a smooth vector field. Let m denote Lebesgue measure, normalised so that $m(M) = 1$. We consider the ODE

$$\dot{x} = F(x, t). \tag{1}$$

In the case where $F(x, t) = F(x)$, we will call the ODE *autonomous*, otherwise we call it *nonautonomous* or *time-dependent*. Let $\phi_\tau : M \times \mathbb{R} \to M$ be the flow, i.e. $\phi_\tau(x_0, t_0)$ is a solution to the ODE (1) with initial condition $x(t_0) = x_0$ and satisfies

$$\frac{\mathrm{d}\phi_\tau}{\mathrm{d}\tau}(x_0, t_0)|_{\tau=0} = F(x_0, t_0), \quad \text{for all } x_0 \in M,\ t_0 \in \mathbb{R}. \tag{2}$$

If a trajectory is at $x_0 \in M$ at time t_0, then τ time units later, the trajectory is at $\phi_\tau(x_0, t_0)$.

Remark 1. In this contribution we will mainly deal with autonomous systems. For this reason and to simplify notation we will state all definitions and theoretical results in terms of an autonomous flow map $\phi_\tau(x) := \phi_\tau(x, 0) = \phi_\tau(x, t)\ \forall t \in \mathbb{R}$. In the fourth case study of a periodically driven velocity field we will directly apply these concepts to the time-dependent flow map $\phi_\tau(x, t)$.

Definition 1. We will call a set $A \subset M$ *invariant* if $\phi_{-\tau}(A) = A$ for all $\tau \in \mathbb{R}$.

Definition 2. Endow M with the Borel σ-algebra and let μ be a probability measure on M. We call μ an *invariant measure* for ϕ if $\mu(\phi_{-\tau}(A)) = \mu(A)$ for all measurable $A \subset M$ and all $\tau \in \mathbb{R}$.

Definition 3. Let μ be an invariant probability measure on M and $A \subset M$ a measurable set. We call μ an *ergodic measure* for ϕ if whenever $\phi_{-\tau}(A) = A$ for all $\tau \in \mathbb{R}$, then either $\mu(A) = 0$ or $\mu(A) = 1$.

The settings we consider will fall into several different classes. We make a distinction between autonomous and time-periodic flows, those in 2D and those in 3D, and those for which the flow is fluid-like (divergence free) or dissipative (negative divergence). We will denote by Λ the "maximal invariant set". In fluid-like flows, $\Lambda = M$, the entire compact domain; for dissipative flows, $\Lambda \subset M$, for example, $\Lambda_0 := \bigcap_{\tau \geq 0} \phi_\tau(M)$ may be a chaotic attractor.

Briefly, our four settings are:

1. *Autonomous fluid-like 2D flow (steady double-gyre flow):* We consider an autonomous flow with a double-gyre pattern. The model is a time-independent version of the double-gyre flow analysed in [11]. The domain $M = [0, 2] \times [0, 1]$ is invariant and so $\Lambda = M$. The flow preserves Lebesgue measure m, which is not ergodic. This example will be used throughout the text to illustrate several fundamental concepts.
2. *Autonomous 3D fluid-like flow (steady ABC flow):* We consider an Arnold–Beltrami–Childress (ABC) flow on a compact domain. Restricting the dynamics to the torus $M = \mathbb{T}^3$ the domain is invariant so $\Lambda = M$. The flow preserves Lebesgue measure m, which is not ergodic. The steady ABC flow is our first case study, which illustrates how the transfer operator approach can be used to detect and approximate invariant sets.
3. *Autonomous 3D dissipative chaotic flows (Lorenz flow and Chua circuit):* These flows are models of convection rolls [31] and of a simple electronic circuit [32], respectively. In both cases the domain M is a neighbourhood of the origin in $\mathbb{R}^3$ and $\Lambda \subsetneq M$ numerically appears to be a chaotic attractor. The flow numerically appears to preserve an ergodic physical invariant measure[1] μ. The Lorenz flow and the Chua circuit are our second and third case studies.
4. *Nonautonomous 2D fluid-like flow (unsteady double-gyre flow):* This time-periodic flow is introduced in [11] and serves as a simplified model of the double-gyre pattern that can be observed in many realistic flows. The domain $M = [0, 2] \times [0, 1]$ is invariant and so $\Lambda = M$. At all times $t \in \mathbb{R}$, the flow preserves Lebesgue measure m, which numerically appears to be not ergodic. The unsteady double-gyre flow is our fourth case study.

In the case studies we will concentrate our analysis on the Lorenz system and the double-gyre flow, while the ABC flow and the Chua circuit will be discussed only briefly.

3. Transfer operators and almost-invariant sets

In this section, we briefly recount some of the background relevant to almost-invariant sets, define the Perron–Frobenius operator, and describe how transfer operator constructions can be used to identify invariant and almost-invariant sets.

Definition 4. Let μ be preserved by ϕ. We will say that a set $A \subset M$ is *almost-invariant* over the interval $[0, \tau]$ if

$$\rho_{\mu,\tau}(A) := \frac{\mu(A \cap \phi_{-\tau}(A))}{\mu(A)} \approx 1. \tag{3}$$

If $A \subset M$ is *almost-invariant* over the interval $[0, \tau]$, then the probability (according to μ) of a trajectory leaving A at some time in $[0, \tau]$ and not returning to A at time τ is relatively small. Thus, almost-invariant sets can be considered as an alternative type of coherent structures in flows.

In the context of analysing a particular flow, we are interested in those sets that are *maximally* almost-invariant; that is, the ratio in Definition 4 is closest to unity. In order to maximise this ratio, one may construct an optimisation problem where the "variables" are sets [16,17]. However, even a spatially discretised version of this optimisation problem is combinatorially hard to solve, and in practice we adopt a heuristic approach to identifying large maximally almost-invariant sets. This heuristic approach utilises eigenfunctions of the Perron–Frobenius operator. The use of the Perron–Frobenius operator has many additional advantages as it is a global linear propagator for the flow and carries significant statistical information on ergodicity and mixing properties [33], and on invariant densities and rates of decay of correlations [33–35].

Definition 5. We define the *Perron–Frobenius operator* or *transfer operator* $\mathcal{P}_\tau : L^1(M) \circlearrowleft$ by

$$\mathcal{P}_\tau f(x) = f(\phi_{-\tau}(x)) \cdot |\det(D\phi_{-\tau}(x))|, \tag{4}$$

where $D\phi_\tau(x)$ is the Jacobian matrix corresponding to the spatial derivatives of ϕ_τ.

If f is the density of an absolutely continuous probability measure ν (so that $\mathrm{d}\nu/\mathrm{d}x = f$), then $\mathcal{P}_\tau f$ is the density of the probability measure $\nu \circ \phi_{-\tau}$.[2] Fixed points of $\mathcal{P}_\tau$ represent densities that are invariant under the action of $\phi_{-\tau}$. If, for example, the flow ϕ is area preserving then $f \equiv 1$ is a fixed point of $\mathcal{P}_\tau$ for all τ. In the autonomous setting, if Lebesgue measure is also ergodic for $x \mapsto \phi_\tau(x)$ for a particular τ, then $f \equiv 1$ is the unique density fixed by $\mathcal{P}_\tau$ Theorem 4.2.2 [33]. If, on the other hand, Lebesgue measure is not ergodic, then $\mathcal{P}_\tau$ will have two or more fixed densities of the form $(1/m(A))\chi_A$ where A is invariant under ϕ (see e.g. the proof of Theorem 4.2.2 [33]). We illustrate these basic concepts in the following simple example.

Example 1 (*Autonomous Double-Gyre*). Consider the two-dimensional autonomous ODE defined by

$$\begin{aligned} \dot{x} &= -\pi \sin(\pi x) \cos(\pi y) \\ \dot{y} &= \pi \cos(\pi x) \sin(\pi y) \end{aligned} \tag{5}$$

on the domain $M = [0, 2] \times [0, 1]$. This autonomous ODE has been constructed from a snapshot of the nonautonomous double-gyre system [11]. There is no transport between the left-hand square $[0, 1] \times [0, 1]$ and the right-hand square $[1, 2] \times [0, 1]$. Each square is foliated with periodic orbits centred about one of the points $(1/2, 1/2)$ and $(3/2, 1/2)$; see Fig. 2. The flow preserves Lebesgue

[1] We will say that the autonomous flow $\phi_\tau(x)$ possesses a *unique physical measure* μ if $\mu_x = \mu$ for Lebesgue almost all $x \in M$, where $\mu_x := \lim_{\tau\to\infty} \frac{1}{\tau} \int_0^\tau \delta_{\phi_s(x)}\,\mathrm{d}s$, and a weak* limit is meant.

[2] This is the natural action of ϕ_τ on a measure ν. Suppose that ν (and f) has its support concentrated on a set A; that is, $\nu(A) = 1$ (and $\int_A f\,\mathrm{d}m = 1$). Then $\nu \circ \phi_{-\tau}(\phi_\tau(A)) = 1$ and $\mathcal{P}_\tau f$ has support on $\phi_\tau(A)$.

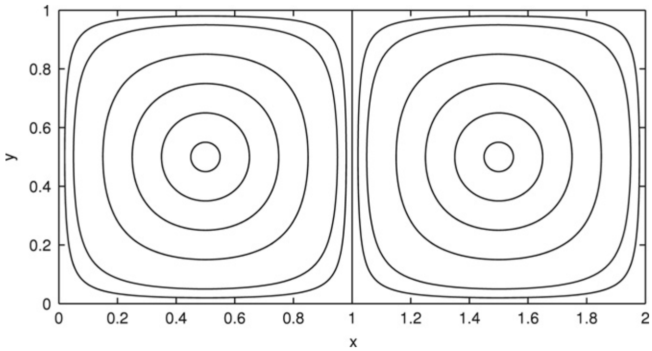

Fig. 2. Typical trajectories in the autonomous double-gyre flow.

measure (normalised so that $m([0,2]\times[0,1]) = 1$) and Lebesgue measure is not ergodic. For example, the left and right squares $[0,1]\times[0,1]$ and $[1,2]\times[0,1]$ are each invariant sets of measure $1/2$. Note that the densities $\chi_{[0,1]\times[0,1]}$ and $\chi_{[1,2]\times[0,1]}$ are both fixed under $\mathcal{P}_\tau$ for all τ.

3.1. Numerical estimation of $\mathcal{P}_\tau$

In order to analyse specific flows with the Perron–Frobenius operator, we require an explicit numerical estimate for $\mathcal{P}_\tau$. A Galerkin approximation known as Ulam's method [36] has been widely used to estimate $\mathcal{P}_\tau$. One partitions M into small connected sets $\{B_1,\dots,B_n\}$ (usually a fine grid of boxes) and applies the projection $\pi_n : L^1(M) \to \mathrm{sp}\{\chi_{B_1},\dots,\chi_{B_n}\}$ defined by

$$\pi_n f = \sum_{i=1}^{n}\left(\frac{1}{m(B_i)}\int_{B_i} f\,\mathrm{d}m\right)\chi_{B_i} \tag{6}$$

to $\mathcal{P}_\tau$ to form $\pi_n\mathcal{P}_\tau$. The action of $\mathcal{P}_\tau$ on $\mathrm{sp}\{\chi_{B_1},\dots,\chi_{B_n}\}$ is given by the matrix[3]

$$P_{n,\tau,ij} = \frac{m(B_i\cap\phi_{-\tau}(B_j))}{m(B_i)}. \tag{7}$$

The matrix $P_{n,\tau}$ is stochastic and therefore has a spectral radius of one and has at least one fixed point[4] p_n (satisfying $p_nP_{n,\tau} = p_n$ and $\sum_{i=1}^n p_{n,i} = 1$), which by the Perron–Frobenius Theorem (see e.g. [37]) is nonnegative. If for a given τ, $x \mapsto \phi_\tau(x)$ preserves an ergodic invariant probability measure μ that is absolutely continuous with respect to Lebesgue measure, then $P_{n,\tau}$ is eventually positive,[5] the eigenvalue 1 is simple, and the corresponding eigenvector p_n is strictly positive; see Proposition 2.3 [38]. An estimate of the (unique) fixed point h of $\mathcal{P}_\tau$ is constructed by setting

$$h_n := \sum_{i=1}^{n}\frac{p_{n,i}}{m(B_i)}\chi_{B_i}. \tag{8}$$

A corresponding approximate invariant probability measure is defined by

$$\mu_n(A) := \int_A h_n\,\mathrm{d}m. \tag{9}$$

Convergence of the peripheral spectrum and eigenprojections of the transition matrix (7) to the true transfer operator as the partition is refined has been considered in a variety of autonomous settings [39–41].

To numerically estimate the fractions in (7), within each B_i, $i = 1,\dots,n$, we will define a set of N test points $x_{i,1},\dots,x_{i,N}$ and numerically integrate trajectories to obtain $\phi_\tau(x_{i,k})$, $k = 1,\dots,N$. Then

$$P_{n;\tau,ij} \approx \frac{\#\{k : x_{i,k}\in B_i,\ \phi_\tau(x_{i,k})\in B_j\}}{N}. \tag{10}$$

The flow time τ should be chosen long enough so that most test points leave their partition set of origin, otherwise at the resolution given by the partition $\{B_1,\dots,B_n\}$, the approximate operator appears similar to the identity operator (i.e. $P_{n,\tau}\approx \mathrm{Id}_{n\times n}$). There is no upper limit on τ, however, if ϕ acts to separate nearby points, clearly the longer τ is, the greater N should be in order to maintain a good representation of the images $\phi_\tau(B_i)$.

3.2. Using eigenvectors to find almost-invariant sets

Let $\mathcal{C}_n := \{A\subset M : A = \bigcup_{i\in I} B_i, I\subset\{1,\dots,n\}\}$. We will search for sets in $\mathcal{C}_n$ that maximise $\rho_{\mu,\tau}$. In practice, we use the following discretised version of ρ:

$$\rho_{n,\tau}(A) := \frac{\sum_{i,j\in I} p_{n,i}P_{n,\tau,ij}}{\sum_{i\in I} p_{n,i}}. \tag{11}$$

We now describe a heuristic method for identifying sets in $\mathcal{C}_n$ for which $\rho_{n,\tau}$ is close to maximal.

Note that the stochastic matrix $P_{n,\tau}$ may be viewed as a transition matrix of an n-state Markov chain. We define a time-reversible version of $P_{n,\tau}$ by

$$R_{n,\tau} := (P_{n,\tau} + \hat{P}_{n,\tau})/2, \tag{12}$$

where $\hat{P}_{n,\tau}$ is the stochastic matrix governing the time reversal of the finite-state Markov chain with transition matrix $P_{n,\tau}$, namely

$$\hat{P}_{n,\tau,ij} = p_{n,j}P_{n,\tau,ji}/p_{n,i}. \tag{13}$$

A simple calculation [17] reveals that (11) is unchanged if $R_{n,\tau}$ is substituted for $P_{n,\tau}$. Thus, for the purposes of calculating $\rho_{n,\tau}$, we henceforth use $R_{n,\tau}$. The following proposition shows that the existence of a set A with $\rho_{n,\tau}(A)\approx 1$ forces the existence of an eigenvalue of $R_{n,\tau}$ close to 1 and vice versa.

Proposition 1. *Let λ_2 denote the second largest eigenvalue of $R_{n,\tau}$ and $A = \bigcup_{i\in I} B_i$, $I\subset\{1,\dots,n\}$.*

$$1-\sqrt{2(1-\lambda_2)} \le \max_{A\in\mathcal{C}_n,\ \sum_{i\in I}p_{n,i}\le 1/2} \rho_{n,\tau}(A) \le \frac{1+\lambda_2}{2}. \tag{14}$$

Proposition 1 is a simple reformulation of Theorem 4.3 [42] in our notation. The proof of the upper bound for $\rho_{n,\tau}$ motivates the following heuristic approach we will use for finding almost-invariant sets. Let $v^2_{n,\tau}$ be the right eigenvector of $R_{n,\tau}$ corresponding to the second largest eigenvalue λ_2 and define the sets

$$A^+ := \bigcup_{i:v^2_{n,\tau,i}\ge 0} B_i,\qquad A^- := \bigcup_{i:v^2_{n,\tau,i}<0} B_i. \tag{15}$$

The pair A^+, A^- partition M into two sets between which we expect little communication of trajectories. This heuristic was originally proposed[6] by Dellnitz and Junge [15,14].

[3] For simplicity of exposition, we will assume throughout that $m(B_i) = m(B_j)$ for all $i\ne j$. If this is not the case, the expression on the RHS of (7) should have $m(B_j)$ in the denominator; the resulting matrix is then not necessarily stochastic. In order to make this matrix stochastic, we can perform a similarity transformation using the diagonal matrix with $m(B_i)$, $i = 1\dots,n$ on the diagonal.

[4] We assume that p_n provides a good estimate of an invariant measure μ via the density h_n(8); see [35] and the references therein for details. As μ does not depend on τ, in practice p_n has negligible time dependence. We will therefore drop the τ dependence for p_n and its corresponding density h_n.

[5] A matrix P is eventually positive if there exists a finite positive integer k such that $P^k > 0$.

[6] Dellnitz and Junge [14] used the left eigenvector $v^2_{n,\tau}$ of $P_{n,\tau}$ corresponding to the second largest eigenvalue λ_2 of $P_{n,\tau}$, and based their heuristic on a perturbation argument; see [14] for details.

Froyland and Dellnitz [16] extended this heuristic by (i) defining

$$A_c^+ := \bigcup_{i:v_{n,\tau,i}^2 \geq c} B_i, \qquad A_c^- := \bigcup_{i:v_{n,\tau,i}^2 < c} B_i, \tag{16}$$

(ii) selecting c so as to maximise $\rho_{n,\tau}(A_c^+)$ and $\rho_{n,\tau}(A_c^-)$, and (iii) by combining the information contained in several eigenvectors that correspond to eigenvalues close to 1. The maximisation over c was based upon elements of the proof of the *lower* bound of Proposition 1, from which the presence of a large second eigenvalue of $R_{n,\tau}$ forces the existence of an almost-invariant set. This dynamical separation procedure is similar in spirit to spectral methods used to decompose graphs, such as described in e.g. [43]. The use of $R_{n,\tau}$ in place of $P_{n,\tau}$ was developed in [17]; in the present work this is the approach we take. In summary:

Algorithm 1.

1. Partition the state space M into a collection of connected sets $\{B_1, \dots, B_n\}$ of small diameter.
2. Construct the Ulam matrix $P_{n,\tau}$ (7) according to (10).
3. Compute the unique fixed left eigenvector p_n of $P_{n,\tau}$ and construct the matrix $\hat{P}_{n,\tau}$ according to (13).
4. Compute $R_{n,\tau}$ using (12) and compute the second largest eigenvalue $\lambda_2 < 1$ and corresponding right eigenvector $v_{n,\tau}^2$.
5. Form A_c^+, A_c^- using (16), selecting c so as to maximise $\min\{\rho_{n,\tau}(A_c^+), \rho_{n,\tau}(A_c^-)\}$.

The choice of maximising $\min\{\rho_{n,\tau}(A_c^+), \rho_{n,\tau}(A_c^-)\}$ is motivated by the following results.

Proposition 2. *Let $\{A^+, A^-\}$ partition M. Then $\rho_{\mu,\tau}(A^+) < \rho_{\mu,\tau}(A^-)$ iff $\mu(A^+) < \mu(A^-)$.*

Proof. Note that

$$1 = \frac{\mu(A^+ \cap \phi_{-\tau}(A^+)) + \mu(A^+ \cap \phi_{-\tau}(A^-))}{\mu(A^+)}$$
$$= \rho_{\mu,\tau}(A^+) + \frac{\mu(A^+ \cap \phi_{-\tau}(A^-))}{\mu(A^+)}, \tag{17}$$

and

$$1 = \frac{\mu(A^- \cap \phi_{-\tau}(A^-)) + \mu(A^- \cap \phi_{-\tau}(A^+))}{\mu(A^-)}$$
$$= \rho_{\mu,\tau}(A^-) + \frac{\mu(A^- \cap \phi_{-\tau}(A^+))}{\mu(A^-)}. \tag{18}$$

Further, note that

$$\mu(A^+ \cap \phi_{-\tau}(A^+)) + \mu(A^+ \cap \phi_{-\tau}(A^-)) = \mu(A^+), \tag{19}$$

and

$$\mu(A^+ \cap \phi_{-\tau}(A^+)) + \mu(A^- \cap \phi_{-\tau}(A^+))$$
$$= \mu(\phi_{-\tau}(A^+)) = \mu(A^+). \tag{20}$$

Equalities (19) and (20) together yield

$$\mu(A^- \cap \phi_{-\tau}(A^+)) = \mu(A^+ \cap \phi_{-\tau}(A^-)). \tag{21}$$

Making the substitution from (21) in Eq. (18) we obtain

$$\rho_{\mu,\tau}(A^+) + \frac{\mu(A^+ \cap \phi_{-\tau}(A^-))}{\mu(A^+)} = \rho_{\mu,\tau}(A^-) + \frac{\mu(A^+ \cap \phi_{-\tau}(A^-))}{\mu(A^-)},$$

from which the result follows. □

Corollary 1. *For any $c \in \mathbb{R}$,*

$$\min\{\rho_{\mu,\tau}(A_c^+), \rho_{\mu,\tau}(A_c^-)\} = \begin{cases} \rho_{\mu,\tau}(A_c^+), & \text{if } \mu(A_c^+) \leq 1/2; \\ \rho_{\mu,\tau}(A_c^-), & \text{if } \mu(A_c^-) < 1/2. \end{cases}$$

Proof. Immediate from Proposition 2. □

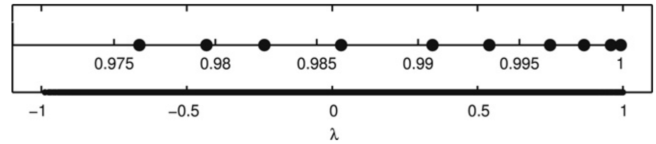

Fig. 3. Ten largest eigenvalues of R_n, each with multiplicity 2 (upper points), where $n = 16384$. Entire spectrum of R_n in the autonomous double-gyre flow (lower strip).

Thus in Step 5 of Algorithm 1 by selecting a value of c to maximise $\min\{\rho_{\mu,\tau}(A_c^+), \rho_{\mu,\tau}(A_c^-)\}$, Corollary 1 guaranteesthat whichever set A_c^+ or A_c^- has the lower ρ value also has μ-mass less than 1/2 and thus the bound of Proposition 1 applies.

Remark 2. In the following, to simplify notation, the index τ will be dropped whenever the flow duration is clear, i.e. P_n denotes $P_{n,\tau}$.

Remark 3. The eigenvectors of R_n will rank invariant and almost-invariant sets according to how "leaky" they are. That is, if one orders the eigenvalues of R_n as $1 = \lambda_1 > \lambda_2 > \lambda_3 > \cdots$, then the sets identified by an eigenvector v_n^k of λ_k using (16) are less leaky than those identified by an eigenvector v_n^m with $m > k$; see [44] for a formal statement. In fact, the eigenvectors v_n^k, $k = 1, \dots, n$ are pairwise orthogonal under the p_n-weighted inner product $\langle v, x\rangle_{p_n} := \sum_{i=1}^n v_i w_i p_{n,i}$ (see e.g. [42, Chapter 6.2.1]). Thus each eigenvector provides information on different almost-invariant sets. In the present paper we focus on the eigenvector v_n^2 and relate the associated almost-invariant sets to invariant manifolds. We refer the reader to [16,44,17,45] for discussion on further subdominant eigenvectors.

Example 2. Continuing with Example 1, we partition $M = [0, 2] \times [0, 1]$ into $n = 16384$ boxes and estimate $\mathcal{P}_\tau$ from (5) and (10) with $\tau = 0.2$. Each box is sampled uniformly with 400 points and the 16384×16384 matrix P_n is constructed. We form $\hat{P}_n$ and R_n via (12) and (13), and compute the outer spectrum of R_n. The spectrum of the matrix R_n, including a zoom of a neighbourhood of 1, is shown in Fig. 3.

We note that the eigenvalue 1 has multiplicity 2. There are two eigenvectors spanning the corresponding eigenspace. One of these eigenvectors is the invariant density $h \equiv 1/2$, and the other is the zero mean function $h_2(x) := \begin{cases} 1/2, & 0 \leq x < 1/2 \\ -1/2, & 1/2 \leq x < 1, \end{cases}$ identifying each half of the domain as an invariant set.

In this example, since the "second" eigenvalue λ_2 equals 1, the bounds (14) force the existence of a subset $A \subset [0, 2] \times [0, 1]$ with $\rho_n(A) = 1$. There are two such sets, namely $[0, 1] \times [0, 1]$ and $[1, 2] \times [0, 1]$ each of which is a union of partition elements from $\{B_1, \dots, B_{16384}\}$.

Remark 4. In Example 2, the partition sets were aligned to the boundaries of the two invariant sets $[0, 1] \times [0, 1]$ and $[1, 2] \times [0, 1]$ and these invariant sets could be constructed as unions of partition elements. In general, however, this may not be the case and the spatial discretisation will destroy invariant sets unless the partition boundaries are adapted to the boundaries of the invariant sets. Thus, a matrix $P_{n,\tau}$ may be ergodic (viewed as a Markov chain) even when $\phi_\tau(\cdot)$ is not transitive. Any *true* positive measure invariant sets of $\phi_\tau(\cdot)$ should be detected as almost-invariant sets via (16) with corresponding eigenvalues extremely close to 1. Furthermore, we expect these eigenvalues to converge to 1 as $n \to \infty$.

This is in contrast to true almost-invariant sets, for which the corresponding eigenvalues bound the "probability of leakage" from sets (via (14)). In this case we expect the eigenvalues to converge to numbers strictly less than 1.

4. Invariant manifolds and almost-invariant sets

The transfer operator approach is a probabilistic view of dynamics. The classical geometric approach to analysing flows is through the study of equilibria, periodic orbits, and invariant manifolds.One of our main aims is to demonstrate that the transfer operator approach is often compatible with this classical approach and that by combining the two approaches, one obtains an even sharper analysis of a system. In this section, we briefly review how invariant manifolds determine invariant sets in fluid-like flows and discuss how these geometric objects can play a role in defining almost-invariant sets in chaotic dissipative systems.

4.1. Invariant manifolds and Lagrangian coherent structures

Consider the autonomous ordinary differential equation $\dot{x} = F(x)$, $x \in M \subset \mathbb{R}^n$, $t \in \mathbb{R}$, and its flow ϕ. Let $\bar{x} \in M$ be a hyperbolic fixed point. Smooth local stable and unstable manifolds of $\bar{x}$ which are tangential to the stable and unstable eigenspaces of $DF(\bar{x})$ exist according to the Stable Manifold Theorem (see e.g. [46], Thm. 1.3.2). In the local stable manifold $W^s_{loc}(\bar{x})$ contraction is exponential with rates given by the real parts of the stable eigenvalues of $DF(\bar{x})$, likewise for the unstable manifold $W^u_{loc}(\bar{x})$ if the system is considered under time reversal. The global stable and unstable manifolds are defined as

$$\begin{aligned} W^s(\bar{x}) &= \{y \in M \mid \lim_{t\to\infty} \phi_t(y) = \bar{x}\} \\ &= \bigcup_{t\geq 0} \phi_{-t}(W^s_{loc}(\bar{x})) \end{aligned} \tag{22}$$

$$\begin{aligned} W^u(\bar{x}) &= \{y \in M \mid \lim_{t\to\infty} \phi_{-t}(y) = \bar{x}\} \\ &= \bigcup_{t\geq 0} \phi_{t}(W^u_{loc}(\bar{x})) \end{aligned} \tag{23}$$

respectively.

In general, invariant manifolds cannot be obtained analytically. However, (22) and (23) suggest a numerical scheme for the approximation of these objects: starting from the local manifolds (which can be approximated in terms of eigenspaces) one obtains the global stable and unstable manifolds by looking at the preimages and images of these local objects, respectively. A variety of numerical algorithms are based on this idea (see [47] for a survey) and we will in particular use the set-oriented continuation scheme introduced in [48], see also [49,50] for details.

We note that stable and unstable manifolds of hyperbolic fixed points or periodic orbits often can also be characterised from a variational point of view. The exponential contraction/expansion near the fixed point and Palis' Lambda-Lemma (see e.g. [46], Thm. 5.2.10) suggest that pairs of points straddling a stable manifold will typically separate exponentially fast, likewise for the unstable manifold when the system is considered under time-reversal (see e.g. [51] for a detailed treatment). In nonlinear[7] systems such exponential behaviour distinguishes these initial conditions from other arbitrary pairs of points. Hence, candidate manifolds can be detected by searching for such distinguished initial conditions. However, if the vector field $F(x, t)$ is time-varying, time-asymptotic structures such as stable and unstable manifolds may not exist. Nevertheless, so-called *Lagrangian coherent structures* (LCS) have been defined [7,8,11], using the variational view described above. A quantity that measures the exponential divergence of infinitesimal perturbations is the *finite-time Lyapunov exponent*:

Definition 6 (*Finite-Time Lyapunov Exponent*). Let $\dot{x} = F(x, t)$ be a nonautonomous ODE with flow ϕ_τ. Fix initial time $_0$ and flow time τ and denote by $D\phi_\tau(x_0, t_0)$ its spatial derivative at x_0. Define

$$\mathcal{E}_\tau(x_0, t_0) = \frac{1}{2\tau} \log(\lambda_{\max}(D\phi_\tau(x_0, t_0)^\top D\phi_\tau(x_0, t_0))), \tag{24}$$

where $\lambda_{\max}(D)$ is the largest eigenvalue of a matrix D. The argument of $\lambda_{\max}$ in (24) is symmetric and $\mathcal{E}_\tau(x_0, t_0)$ represents the largest relative length growth of any vector under the action of $D\phi_\tau(x_0, t_0)$. $\mathcal{E}_\tau(x_0, t_0)$ is called the largest finite-time Lyapunov exponent associated with the trajectory $\phi_s(x_0, t_0)$, $s \in [0, \tau]$. For the time-reversed system we define

$$\begin{aligned} \bar{\mathcal{E}}_\tau(x_0, t_0) &:= \mathcal{E}_{-\tau}(x_0, t_0) \\ &= \frac{1}{2\tau} \log(\lambda_{\max}(D\phi_{-\tau}(x_0, t_0)^\top D\phi_{-\tau}(x_0, t_0))). \end{aligned} \tag{25}$$

So-called "ridges" in the scalar fields $\mathcal{E}_\tau(x_0, t_0)$ or $\bar{\mathcal{E}}_\tau(x_0, t_0)$ indicate the location of repelling and attracting LCS [7,8,11,12]. In the autonomous setup considered in Sections 5–7 LCS can be viewed as an approximation of the classical invariant manifolds (see e.g. [11,12]). The same applies for the Poincaré return map of the periodically driven flow in Section 8.

In Sections 5, 7 and 8 we estimate stable and unstable manifolds by applying a set-oriented methodology [51] to Definition 6. A box-valued approximation of the finite-time Lyapunov exponent field is computed; for each box in the covering $\{B_1, \ldots, B_n\}$ we define the expansion rate of a box B_i, $i = 1, \ldots, n$, as

$$\delta_\tau(B_i, t) := \max_{x\in B_i} \mathcal{E}_\tau(x, t), \tag{26}$$

and

$$\bar{\delta}_\tau(B_i, t) := \max_{x\in B_i} \bar{\mathcal{E}}_\tau(x, t), \tag{27}$$

respectively.

Each box carries local upper bounds for the two FTLE fields. If the box shrinks to a point x then via the continuity of the FTLE fields the quantities $\mathcal{E}_\tau(x, t)$ and $\bar{\mathcal{E}}_\tau(x, t)$ are recovered. In practice, the expansion rates (26) and (27) are approximated using a collection of uniformly distributed initial conditions in each box and taking the maximum in (26) and (27) with respect to these points. The individual $\mathcal{E}_\tau(x, t)$ and $\bar{\mathcal{E}}_\tau(x, t)$ are either computed by solving the variational equation as in Eqs. (24) and (25), or alternatively via computing the growth rate of the relative distance of pairs of particle trajectories. The latter approach has the advantage that it is derivative free and is therefore particularly suitable when the Jacobian is difficult to obtain, for instance when the RHS of the ODE is only given in terms of discrete data. Accuracy of the approximation is ensured by sufficiently small initial perturbations and sufficiently fine sampling. More details on the set-oriented expansion rate approach and convergence statements can be found in [51].

4.2. Autonomous flows in two dimensions

Invariant manifolds of autonomous flows on compact surfaces form impenetrable barriers for trajectories. If unions of segments of invariant manifolds form a closed curve, then the region enclosed by this curve is an invariant set. In this way, the invariant manifolds form a skeleton of the dynamics, dividing the domain into uncommunicating regions. In the autonomous double-gyre of Example 1, taking a geometric approach, we note that there is a heteroclinic connection of the unstable manifold of the fixed point $(1, 1)$ and the stable manifold of the fixed point $(1, 0)$. This invariant manifold separates the two halves of the domain M into the invariant sets $[0, 1] \times [0, 1]$ and $[1, 2] \times [0, 1]$. Taking a transfer operator approach, the two invariant sets $[0, 1] \times [0, 1]$ and $[1, 2] \times [0, 1]$ can be detected by the second eigenvector of R_n. Thus the

[7] In a linear system almost all pairs of initial conditions will separate exponentially at the same rate. The only exceptions are those pairs that are exactly aligned with the stable direction.

maximally almost-invariant sets can be easily identified via the eigenfunction of the transfer operator corresponding to the second largest eigenvalue. We remark that the separating heteroclinic orbit would also be clearly detected by both fields $\mathcal{E}_t$ and $\bar{\mathcal{E}}_t$.

To conclude we point out that the other major geometric structures, namely the family of invariant sets enclosed by foliations of periodicorbits shown in Fig. 2 are also detected by combining eigenfunctions corresponding to the second and third largest eigenvalues of the transfer operator.

4.3. Autonomous fluid-like flows in three dimensions

The situation in three dimensions is more complicated. Studies of fluid-like flows on compact domains such as the Arnold–Beltrami–Childress (ABC) flow, defined by (29), have shown that there can exist invariant tori that divide the phase space into invariant sets. For example, [52] prove that for small positive C in (29) the ABC flow possesses invariant tori. However, the numerical identification of these invariant tori and associated invariant sets can be difficult. Haller [8] has employed hyperbolicity times and finite-time Lyapunov exponents to obtain numerical estimates of the 2D stable and unstable manifolds of hyperbolic periodic orbits that appear to bound invariant regions identified by Dombre et al. [53]. In our first case study, in Section 5, we demonstrate that these invariant regions are identified via our transfer operator approach and are easily extracted from the eigenvectors of the associated matrix R_n.

4.4. Autonomous dissipative flows in three dimensions

For chaotic dissipative flows, such as the Chua [32] and Lorenz [31] flows (see Sections 6 and 7 for definitions), Lebesgue almost all trajectories starting in a neighbourhood of the attractors appear numerically to exhibit a unique ergodic invariant measure. In fact, Tucker [54] has shown that the Lorenz system has a unique SBR measure μ and by ergodicity of μ there are no invariant sets with μ-measure strictly between 0 and 1. Nevertheless *almost*-invariant sets may exist for such flows and we can ask where these sets lie in phase space and what relationship they have to invariant manifolds. We demonstrate in two case studies, in Sections 6 and 7, that there is a very close connection between almost-invariant sets and primary intersections of stable and unstable manifolds of equilibrium points and low-period unstable periodic orbits of the flow. Studies of almost-invariant sets for the Chua and Lorenz systems have been undertaken in [15,16] respectively, however the linking of these probabilistic findings with the geometry of invariant manifolds is completely new.

4.5. Periodically driven fluid-like flows in two dimensions

In periodically driven fluid-like flows such as the double-gyre flow [11] (see Section 8) stable and unstable manifolds of hyperbolic periodic orbits typically intersect transversally giving rise to horseshoe dynamics. Nonetheless closed curves composed of segments of stable and unstable manifolds form partial barriers to transport where the heteroclinic tangle provides the transport mechanism across the boundary. This concept is known as lobe dynamics (see e.g. [5,6,3]) and has been successfully applied in a variety of settings. In addition to chaotic motion induced by the horseshoe dynamics, in the double-gyre system we can observe regions of regular motion such as invariant tori. The transfer operator approach picks up regions formed by families of invariant tori as the most almost-invariant sets. The transfer operator approach also identifies almost-invariant sets with *non-invariant* boundaries close to the manifolds responsible for the heteroclinic tangle.

4.6. Connecting the probabilistic and geometric approaches

The connection between the probabilistic and geometric approaches is most clear when there is a positive volume region A bounded by unions of invariant manifolds (e.g. the steady double-gyre and the steady ABC flow). Impenetrability of the manifolds means that A is invariant and so $\chi_A/m(A)$ is an eigenfunction of $\mathcal{P}_\tau$. The connection between the probabilistic and geometric approaches is less clear when no such invariant set exists.

Let us first discuss the setting of Sections 6 and 7 which study the Lorenz and Chua systems respectively. The attracting set of the Lorenz system is known to be transitive [54], and there is numerical evidence that the attracting set of the Chua system is also transitive. The dynamics occurs on the unstable manifolds that comprise the chaotic attractor. By transitivity, it is impossible to enclose an open invariant set in the attractor by segments of stable manifold. Nevertheless, there is still the possibility that *almost*-invariant sets exist and the geometrical nature of the boundaries of globally maximal almost-invariant sets may be non-trivial.

Definition 7. Consider a positive d-dimensional volume connected set $A \subset M \subset \mathbb{R}^d$. We call the *regular* part of the boundary ∂A of A that portion of ∂A that may be represented as a finite union of segments of co-dimension 1 invariant manifolds, with each segment having positive $(d-1)$-dimensional volume. The remainder of ∂A we will call an *exit boundary*.

In Sections 6 and 7 we demonstrate that the boundaries of globally maximal almost-invariant sets as determined by the transfer operator formalism are mostly comprised of stable manifolds. The remaining part of the boundary is not aligned with a stable manifold and it is only through this piece of the boundary, which we term an "exit boundary", that transport is possible. We conjecture that this is a universal way in which almost-invariant sets are formed: by bounding them with segments of stable manifold and leaving a small exit boundary through which trajectories may leave the almost-invariant set.

We now argue heuristically that if one continuously deforms the boundary of an almost-invariant set A away from a stable manifold, the invariance ratio will decrease. We thus argue that *local* maxima of $\rho_{\mu,\tau}(A)$ are obtained by matching a segment of the boundary of A with a stable manifold.

We begin by noting that

$$\rho_{\mu,\tau}(A) = \frac{\mu(A \cap \phi_{-\tau}(A))}{\mu(A)} = \frac{\mu(\phi_\tau(A) \cap A)}{\mu(A)}, \tag{28}$$

as ϕ_τ is invertible and preserves μ. We consider the locally 2D setting where our set A is contained in a locally 2D attractor Λ; similar arguments apply in a 3D setting. Suppose that there exists a stable manifold $W^s(x_0)$ of a hyperbolic fixed point x_0 and denote by C the intersection of some segment $\mathcal{W}$ of this manifold with Λ. Suppose also that there exists an almost-invariant set A in the vicinity of C, but not intersecting C; see Fig. 4(a).

Consider the local effect on points in A near C. By hyperbolicity, in backward time, points in A near C will be attracted out of A toward C; see Fig. 4(a). If A were to enlarge to cross C, those points in A on the right of C would be repelled from C and would leave A; see Fig. 4(b). However, by locally matching precisely the boundary of A with C both of these effects can be eliminated, reducing the loss of points from A locally near C in both backward and forward time, and increasing the value of $\rho_{\mu,\tau}(A)$. Thus, heuristically, we argue that if one continuously deforms the boundary of an almost-invariant set A away from a stable manifold, $\rho_{\mu,\tau}(A)$ will decrease and $\rho_{\mu,\tau}(A)$ will have a local maximum when the boundary of A precisely matches the segment C.

Finding the *globally* maximal almost-invariant sets is highly non-trivial, and practically impossible using only estimates of

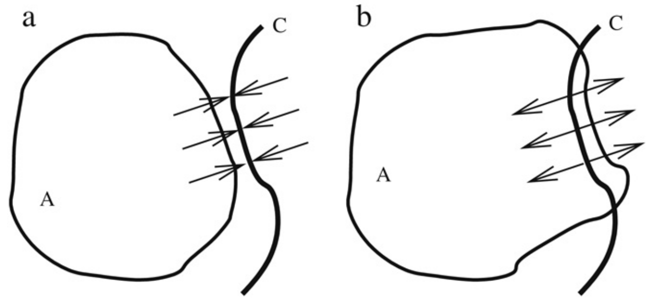

Fig. 4. (a) Almost-invariant set A in a locally 2D attractor Λ with boundary near $C = \mathcal{W} \cap \Lambda$ where $\mathcal{W} \subset W^s(x_0)$ is a locally 1D segment of a stable manifold $W^s(x_0)$ of a hyperbolic fixed point x_0. In reverse time, points in A near C are attracted out of A toward C. (b) Almost-invariant set A crossing $C = \mathcal{W} \cap \Lambda$. In forward time, those points in A on the right of C are repelled out of A. Both of these effects are minimised when the boundary of A matches C.

invariant manifolds. It is far from clear *which* stable manifold segments one should piece together to form a globally maximal almost-invariant set. In Sections 6 and 7 we find that these boundaries are formed from stable manifolds of fixed points or low period orbits. We also find that these stable manifolds are associated with the strongest "ridges" in an FTLE field. One may be tempted to conjecture that globally maximal almost-invariant sets have boundaries formed from stable manifolds associated with the strongest "ridges" in an FTLE field. However, while local deviation of boundaries from such stable manifolds would lead to rapid flux across the new boundary, as argued in Fig. 4, the *global* structure of the manifolds and the *size* and *position* of the exit boundary also play a role.

In Section 8 we show that the global maximum of $\rho_{\mu,\tau}$ does not correspond to a set bounded by stable or unstable manifolds. In this case, we have a boundary with a rather large "exit boundary", but an exit boundary that is well placed with respect to the dynamics so that mass transfer through the exit boundary is very small.

5. Case Study I — Autonomous fluid-like 3D flow (ABC flow)

To illustrate our methodology we begin with the following 3D system of ordinary differential equations:

$$\begin{aligned}\dot{x} &= A\sin z + C\cos y\\ \dot{y} &= B\sin x + A\cos z\\ \dot{z} &= C\sin y + B\cos x.\end{aligned} \tag{29}$$

This class of flows is known as ABC (Arnold–Beltrami–Childress) flows and the system (29) is notable for being an exact steady solution of Euler's equation, exhibiting a nontrivial streamline geometry. We refer the reader to Haller [8] for a numerical analysis, and to Dombre et al. [53] for an analytical investigation. As in [53] we consider the ABC flow on the torus $\mathbb{T}^3$, i.e. $0 \le x, y, z < 2\pi$ in (29). The domain is invariant and preserves Lebesgue measure. For our choice of parameters $A = \sqrt{3}$, $B = \sqrt{2}$, $C = 1$ (cf. [8]) theflow is non-integrable and the system exhibits non-trivial invariant sets which are enclosed by 2D invariant manifolds.

The results for the application of the set-oriented expansion rate approach [51] as described in Section 4.1 are shown in Fig. 5(a). Here we used flow time $\tau = 5$ and coloured the boxes B_i from a very fine box discretisation according to $\max\{\delta_\tau(B_i), \bar{\delta}_\tau(B_i)\}$. High values in the scalar field highlight stable and unstable invariant manifolds of hyperbolic periodic orbits and confirm Haller's results [8]. Moreover the picture gives an indication of the dynamically distinct regions in the ABC flow.

For the numerical approximation of the transfer operator we partition $M = [0, 2\pi]^3$ into $n = 262144 = 2^{18}$ boxes and estimate $\mathcal{P}_\tau$ from (10) with $\tau = 0.2$. Each box is sampled uniformly with 1000 points and the 262144×262144 sparse matrix P_n is constructed. We form $\hat{P}_n$ and R_n via (13) and (12), and compute the outer spectrum of R_n. The largest six eigenvalues $\lambda_1 = 1$, $\lambda_2 = 0.9986$, $\lambda_3 = 0.9979$, $\lambda_4 = 0.9978$, $\lambda_5 = 0.9971$, and $\lambda_6 = 0.9968$ are very close to 1. The eigenvector for the eigenvalue $\lambda_1 = 1$ gives the uniform invariant density, while the eigenvectors v_n^i, $i \ge 2$, characterise almost-invariant sets, see Fig. 5(b). In fact these sets are truly invariant, the leakage is only due to the numerical discretisation described above; see Remark 4. For a finer discretisation the leading eigenvalues will converge to one and, consequently, the corresponding eigenvectors will relate to invariant sets. We note that the numerical results are very robust in that sense that the leading eigenvectors with respect to a coarser partition of M highlight the same regions.

In order to extract approximations of some of the large invariant sets enclosed by invariant manifolds, we apply the heuristic approach described in Algorithm 1 to the eigenvector v_n^2.

The resulting partition into three sets is shown in Fig. 6(a). In Fig. 6(a) we also overlay the invariant manifolds obtained via taking regions with high values in the combined forward and backward time FTLE field as described above. These structures align exactly with the set boundaries that result from the thresholding approach. This confirms that truly invariant sets of the flow have been approximated.

Fig. 5. (a) Application of the set-oriented FTLE approach using flow times $\tau = \pm 5$ on the ABC flow model with dark values highlighting invariant manifolds. The scalar field gives an indication of dynamically distinct regions. (b) Extremal values in the eigenvector v_n^2 of R_n, $n = 262144$, in the ABC flow indicate the existence of (numerically almost-)invariant sets.